FOR SUBMISSION TO APJ
Preprint typeset using LaTeX style emulateapj v. 11/10/09

FROM THE BLAZAR SEQUENCE TO THE BLAZAR ENVELOPE: REVISITING THE RELATIVISTIC JET DICHOTOMY IN RADIO-LOUD AGN

EILEEN T. MEYER AND GIOVANNI FOSSATI
Department of Physics and Astronomy, Rice University, Houston, TX 77005

MARKOS GEORGANOPOULOS
Department of Physics, University of Maryland Baltimore County, Baltimore, MD 21250 and
NASA Goddard Space Flight Center, Mail Code 663, Greenbelt, MD 20771, USA

MATTHEW L. LISTER
Department of Physics, Purdue University, West Lafayette, IN 47907
For Submission to ApJ

ABSTRACT

We revisit the concept of a blazar sequence that relates the synchrotron peak frequency ($\nu_{\rm peak}$) in blazars with synchrotron peak luminosity ($L_{\rm peak}$, in νL_ν) using a large sample of radio-loud AGN. We present observational evidence that the blazar sequence is formed from two populations in the synchrotron $\nu_{\rm peak} - L_{\rm peak}$ plane, each forming an upper edge to an envelope of progressively misaligned blazars, and connecting to an adjacent group of radio galaxies having jets viewed at much larger angles to the line of sight. When binned by jet kinetic power ($L_{\rm kin}$; as measured through a scaling relationship with extended radio power), we find that radio core dominance decreases with decreasing synchrotron $L_{\rm peak}$, revealing that sources in the envelope are generally more misaligned. We find population-based evidence of velocity gradients in jets at low kinetic powers ($\sim 10^{42} - 10^{44.5}$ erg s^{-1}), corresponding to FR I radio galaxies and most BL Lacs. These low jet power 'weak jet' sources, thought to exhibit radiatively inefficient accretion, are distinguished from the population of non-decelerating, low synchrotron-peaking (LSP) blazars and FR II radio galaxies ('strong' jets) which are thought to exhibit radiatively *efficient* accretion. The two-population interpretation explains the apparent contradiction of the existence of highly core-dominated, low-power blazars at both low and high synchrotron peak frequencies, and further implies that most intermediate synchrotron peak (ISP) sources are not intermediate in intrinsic jet power between LSP and high synchrotron-peaking (HSP) sources, but are more misaligned versions of HSP sources with similar jet powers.

Subject headings: galaxies: active — galaxies: nuclei — galaxies: jets

1. INTRODUCTION

The success of the current model for radio-loud Active Galactic Nuclei (AGN) as accreting super-massive black holes with bipolar, relativistic jets has rested on the ability of this physical paradigm to successfully explain the chameleon nature of the spectral energy distribution (SED) of this family of extreme objects. The jet model is inherently anisotropic and allows us to unify the highly luminous and variable blazars as relativistically beamed counterparts of Fanaroff-Riley (FR) radio galaxies (Fanaroff & Riley 1974).

The typical blazar spectrum exhibits a double peak (in νF_ν), attributed to synchrotron and inverse Compton (IC) radiation from the relativistic jet, which dominates in blazars due to the alignment of the jet axis near to our line-of-sight (for a review of leptonic blazar models, see Böttcher 2007). The synchrotron component peaks from sub-infrared (IR) energies up to hard X-rays, with the IC component peaking at much higher energies (typically gamma-rays). Spectroscopically, blazars are traditionally divided between optically 'featureless' BL Lac objects and (broad) emission line-emitting Flat Spectrum Radio Quasars (FSRQ). The long-standing orientation-based unification scheme for radio-loud AGN proposes BL Lacs and FSRQ as counterparts to FR I and FR II radio galaxies, respectively, based on similar spectra, morphologies, and range in extended radio luminosity (Urry & Padovani 1995).

However, violations to this scheme are well-known, and findings of powerful, FR II-like BL Lacs, and low-power FSRQ (Landt et al. 2006; Landt & Bignall 2008; Kharb et al. 2010) appear to break the simplest dichotomy (going back to the original FR classification) between the lobe-dominated, high-power FR II galaxies and the low-power, edge-darkened FR Is. Kharb et al. (2010) also found BL Lacs displaying SEDs and hot-spots typical of quasars while others have observed BL Lacs exhibiting broad lines in low continuum states (Vermeulen et al. 1995; Corbett et al. 2000; Raiteri et al. 2007).

Further, the importance of optical spectral type in connecting radio galaxies with their aligned counterparts is difficult to assess due to the strong effects of relativistic beaming on equivalent width measurements on which the blazar classifications are based (Georganopoulos & Marscher 1998; Ghisellini et al. 2010). At the same time, the designation of Low and High Excitation Radio Galaxies (LERG and HERG, cor-

meyer@rice.edu

responding to prominence of emission lines as measured with an excitation index, see Hine & Longair 1979) is increasingly found to be mixed among FR I and FR II morphological types; all of this creates serious problems for a unification scheme which connects spectral type with the morphology.

1.1. *The Blazar Sequence*

The synchrotron peak frequency ($\nu_{\rm peak}$) may take on a wide range of values (from 10^{12} to 10^{18} Hz at the extremes), and is one of the principle ways to classify individual blazars. While FSRQ sources are typically found to have low $\nu_{\rm peak}$ ($< 10^{14.5}$ Hz), BL Lacs are found to span the entire range, with low, intermediate, and high-peaking BL Lacs (LBL, IBL, and HBL) typically dominating surveys selecting in the radio, optical, or X-ray, respectively. We adopt the generic terms for low, intermediate, and high *synchrotron-peaking* (LSP, ISP, HSP) blazars independently of the spectroscopic type, as in Abdo et al. (2010c).

Fossati et al. (1998) found an anti-correlation between the frequency of the synchrotron peak and the bolometric and synchrotron peak luminosities and suggested a link between the power of the source and $\nu_{\rm peak}$. This sequence appeared to match a spectroscopic one, from predominantly powerful FSRQ sources at the low-peak, high-luminosity end through LBLs and finally HBLs, at the low-luminosity end. Ghisellini et al. (1998) suggested that more efficient cooling of particles in the jets of high luminosity blazars is responsible for the lower peak frequencies. However, it is not clear how the continuous blazar sequence fits in with the bi-modality of morphology and spectral type in radio galaxies.

1.2. *Beaming and Quantitative Unification*

Orientation-based unification predicts that misaligned blazars will drop in luminosity and synchrotron peak frequency according to the decrease in Doppler boosting with increasing angle. In the simplest case (a single Lorentz factor and a convex spectrum), the ratio of decrease in log frequency to log luminosity will be approximately 1:4, roughly orthogonal to the sequence. (This holds for moving features in the jet; for a standing shock model the relation is 1:3, see *e.g.*, Lind & Blandford 1985). The connection between blazars and the *nuclear emission* in radio galaxies can naturally inform our jet models. The synchrotron nature of the nuclear radio galaxy emission has been confirmed by comparison of the broad-band spectral indices and SED characteristics of FR I nuclei with BL Lacs (Chiaberge et al. 1999; Capetti et al. 2000; Chiaberge et al. 2000; Capetti et al. 2002; Trussoni et al. 2003), where the effects of relativistic beaming (rather than obscuration) accounted for the $10-10^4$ difference in radio and optical luminosities between the BL Lacs and radio galaxies.

Capetti et al. (2002) and Trussoni et al. (2003) agree upon jet bulk Lorentz factors of $\Gamma \sim 4-6$ in order to account for the difference in radio galaxy and blazar luminosities, while Hardcastle et al. (2003) found $\Gamma \sim 3$ sufficient to match the luminosity functions of the B2 and EMSS and 1 Jy samples. These values agree with VLBI studies of the pc-scale jets of HSP BL Lacs which show that they are barely super-luminal, with average bulk Lorentz factors $\Gamma \sim 2-3$ (Piner et al. 2001; Edwards & Piner 2002; Giroletti et al. 2004; Piner et al. 2008, 2010); however, several LSP BL Lacs show high velocities on VLBI scales (Jorstad et al. 2001; Cohen et al. 2007). Interestingly, Hardcastle et al. (2003) also found that they could not reproduce the redshift distribution of 1 Jy BL Lac sample unless some of the high-redshift BL Lacs corresponded to FR IIs.

In contrast, high Doppler factors ($\sim$ 50 or greater) must be invoked to explain the brightness and rapid variability of TeV blazars, as the jet must be highly relativistic in order to avoid absorption by co-spatial IR photons (Dondi & Ghisellini 1995; Aharonian et al. 2007; Ghisellini et al. 2009; Giannios et al. 2009). The discrepancy in apparent jet speeds and radio galaxy nuclear emission can be resolved at least for FR I/BL Lac sources by invoking the presence of structured jets with multiple emitting regions of varying speeds. This includes the spine-sheath axisymmetric model explored by Swain et al. (1998), Chiaberge et al. (2000), and Ghisellini et al. (2005), and the decelerating model of Georganopoulos & Kazanas (2003), all of which imply a high-speed spine or base which dominates the flux when the source is aligned, and a slower component which dominates if the source is misaligned. Other blazar studies also support the decelerating model for low power blazars, as recent VLBI observations of the MOJAVE sample[1] reveal that the these sources also have lower apparent jet speeds, versus the high-power FSRQ which maintain collimated jets and consistent jet speeds over longer distances (Lister et al. 2009).

1.3. *The Blazar Envelope*

The simplest scenario behind the appearance of a blazar sequence is that the physical properties of extragalactic jets (as measured through the synchrotron peak frequency and luminosity) are a function of a single parameter, the jet kinetic power ($L_{\rm kin}$). If there is a one-to-one correspondence between $\nu_{\rm peak}$ and $L_{\rm kin}$, the original blazar sequence could be seen as the extreme 'edge' of an envelope, consisting of the most aligned (and therefore brightest) objects. More misaligned sources should appear below the sequence, causing it to widen. If the jets are monoparametric in terms of jet power, these misaligned sources should fall in a line away from their aligned counterparts on the sequence, according to the drop in Doppler factor, forming 'tracks' of similar kinetic power in the envelope of blazars populating the $\nu_{\rm peak}$ - $L_{\rm peak}$ plane.

The original blazar sequence was based on 126 objects, a few dozen of which were detected in gamma-rays. Over a decade later there are thousands more blazars and blazar candidates in the literature and a much greater density of multi-wavelength data in general. Many of the newer samples have been designed to combat the early selection effects of the radio and X-ray surveys, such as the low radio power *CLASS* sample (Caccianiga & Marchã 2004), and it is now clear that as our surveys go deeper, many more low-luminosity blazars are emerging. These newer samples challenge both the sequence and its simplest extension that considers the sources in the enve-

[1] MOJAVE (Monitoring Of Jets in Active galactic nuclei with VLBA Experiments): Over 250 bright blazars being continuously monitored with VLBI. (www.physics.purdue.edu/mojave)

TABLE 1
BLAZAR SAMPLES

Sample	Abbrev.	No. of Objects†	References
1 Jansky blazar sample	1 Jy	34	Stickel et al. (1991)
2-degree field (2dF) QSO survey	2QZ	56	Londish et al. (2002, 2007)
2 Jansky survey of flat-spectrum sources	2 Jy	213	Wall & Peacock (1985)
The Candidate Gamma-Ray Blazar Survey	CGRaBS	1625	Healey et al. (2008)
Cosmic Lens All-sky Survey	CLASS	236	Marchã et al. (2001); Caccianiga et al. (2002); Caccianiga & Marchã (2004)
Deep X-ray Radio Blazar Survey	DXRBS	283	Perlman et al. (1998); Landt et al. (2001); Padovani et al. (2007)
EGRET blazar sample	...	555	Mukherjee et al. (1997)
Einstein Slew survey sample of BL Lac objects	...	48	Perlman et al. (1996)
Fermi blazar sample	1FGL	689	Abdo et al. (2010a)
Hamburg-RASS bright X-ray AGN sample	HRX	104	Beckmann et al. (2003)
Parkes quarter-Jansky flat-spectrum sample	...	878	Jackson et al. (2002); Hook et al. (2003); Wall et al. (2005)
Radio-Emitting X-ray source survey	REX	55	Caccianiga et al. (1999)
Radio-Optical-X-ray catalog	ROXA	816	Turriziani et al. (2007)
RASS - Green Bank BL Lac sample	RGB	127	Laurent-Muehleisen et al. (1999)
Einstein Medium-Sensitivity Survey of BL Lacs	EMSS	44	Morris et al. (1991); Rector et al. (2000)
RASS - SDSS flat-spectrum sample	...	501	Plotkin et al. (2008)
Sedentary survey of high-peak BL Lacs	...	150	Giommi et al. (1999, 2005); Piranomonte et al. (2007)

† Number of sources listed is total sources in sample (not necessarily number of blazars).

tended radio luminosity are related. We therefore chose the low-frequency extended luminosity (also commonly referred to as steep or lobe emission) at 300 MHz (L_{300}) as an estimator of the jet power for this work. This value is then converted to L_{kin} from the linear fit (with 1-σ error),

$$\log L_{kin} = 0.64(\pm 0.09)\ (\log L_{300} - 40) + 43.54(\pm 0.12)\ \ [\mathrm{ergs\ s^{-1}}] \quad (1)$$

taken from Cavagnolo et al. (2010). Although the scatter in the scaling is not insignificant ($\sim$ 0.7 decade in L_{kin}), it is adequate for our purpose of classifying sources in broad bins of jet power. This value (L_{kin}) is what we generally refer to throughout the paper as the jet (kinetic) power, not to be confused with L_{peak} or other observables of the jet which are affected by beaming.

2.2.1. *Extended Radio Emission*

The extended radio emission from the lobes of radio galaxies differs from the beamed core emission in being both non-variable and generally exhibiting a much steeper spectrum. Thus one way to isolate the extended emission is to look for a change in the spectral index at low frequencies. For our sample, a spectral decomposition (SD) method was applied to all sources which had data points at five or more frequencies below 10^{11} Hz. Sources were tested for a two-component spectrum by fitting alternately with a double power-law and then a single power law (assuming normal error). Because the latter can be expressed as a particular case of the former, this allowed us to use the maximum likelihood (L) ratio test for nested models. In this test, the statistic $-2\Delta\log(L)$ distribution can be approximated as a χ^2 with n_2 - n_1 degrees of freedom (Wilks 1938). The double power-law model has $n_2 = 4$ degrees of freedom (slope and normalization for each powerlaw), while the null hypothesis model has $n_1 = 2$, for a total of two degrees of freedom. We rejected the two power-law fit for a significance level α >0.05. The best steep-spectrum fit from the hypothesis test was then used to calculate L_{300}.

The normal approximation for the spread around the power law is a rough approximation, and for eight sources it appears the fit failed to find a significant two-powerlaw solution due to a great deal of variability in the radio core points. L_{300} was estimated for these sources by fitting hand-selected low-frequency radio points corresponding to a stable emission component persistent beneath the core variability. This method was also used for a few sources which passed the test, where core variability caused the steep power law fit to be somewhat more flat than would be fit by eye (a correction of a few percent). We note that inclusion of these eight sources and the corrections do not materially affect the results presented.

The SD method is the most reliable way to separate the boosted core emission from the isotropic lobe emission, as it is model independent. Another method is to measure the extended emission from core-subtracted VLA images (typically at 1.4 GHz). In order to expand our sample and counter some selection bias (see longer discussion in §4.2), extended flux measurements were taken from the literature where available (see Table 2 for references). One difficulty with these measurements is that an assumption must be made about the spectral index used to extrapolate from 1.4 GHz to the 300 MHz luminosity. It is also clear from sources with both a visible steep spectrum and VLA data that these are not always in agreement. Even for the same object, VLA estimates by different authors can vary widely, as in the case of 3C 446, with 1.4 GHz extended flux estimates of 91.6, 271, and 4030 mJy (Kharb et al. 2010; Cooper et al. 2007; Antonucci & Ulvestad 1985), none of which agrees with a clear steep component which suggests a flux $\simeq$ 800 mJy at that frequency. However, examination of the over 100 sources with both VLA and SD estimates reveals that

lope simply to be de-beamed blazars. Contrary to what is anticipated by the sequence, Landt & Bignall (2008) showed that HSP and LSP BL Lacs objects cover similar ranges in extended radio power. Caccianiga & Marchã (2004) found several low luminosity, low $\nu_{\rm peak}$ sources with relatively high core dominance compared to brighter objects at similar low $\nu_{\rm peak}$, suggesting that the former are not simply related to the latter through misalignment, as one might naively expect.

In this paper we examine the available evidence for a 'blazar envelope' beneath the upper-limit of the most aligned blazars, due primarily to mis-alignment. We test the possibility that jets are monoparametric engines by examining how the source power is related to other properties of the blazar such as location in the $\nu_{\rm peak} - {\rm L}_{\rm peak}$ plane, and re-evaluate the blazar sequence in light of the great increases in multi-wavelength, multi-epoch data available for blazar and radio galaxy jets.

The paper is organized as follows: in §2 we explain the sample selection and describe our statistical and phenomenological models which allowed us to estimate the important envelope parameters for blazars and radio galaxies. In §3 we present the results of the first round of data collection and analysis and the 'blazar envelope'. In §4 we discuss the implications of the blazar envelope and the potential for constraining jet models. In §5, we summarize our findings. Throughout the paper we adopt a cosmology based on the concordance model with $\Omega_M = 0.27$, $\Omega_\Lambda = 0.73$, and $H_0 = 71$ km s^{-1} Mpc^{-1}. Energy spectral indices are defined such that $f_\nu \propto \nu^{-\alpha}$, and all luminosities ($\rm L_\nu$) are references to powers ($\nu {\rm L}_\nu$ implied).

2. METHODS

In order to investigate the nature of the blazar envelope, we require a sample of blazars with a well-sampled SED such that a reliable estimate of the synchrotron peak location can be made. The scarcity of such blazars may recommend utilizing as many sources as are known without regard for flux-limited samples, but this approach risks losing the ability to understand the limits of our observations. We compromise by combining multiple well-defined (flux-limited) samples of flat-spectrum sources. The overall sample definition is thus complex, but does allow for the examination of biases by population modeling, as discussed in §4.2.

2.1. *The Blazar Sample*

The flat spectrum candidate sample was made from the surveys listed in Table 1. A multi-frequency database of all sources in this master list was compiled by a combination of all the data in the original publications, with additional data from the literature and from the SIMBAD and NED online databases, for a total of 3773 sources (taking into account duplicates). For 69 sources, previously unpublished Swift data were available which were utilized to produce fluxes and X-ray indices. Spectroscopic classification was taken from NED, SIMBAD, or the most recent publication, and non-blazar sources were removed, leaving 3014 blazars. A further reduction was made by removing sources with sparse multi-frequency SED sampling. The minimum required sampling was photometry at 3, 2, and 1 or more unique frequencies for the (rest frame) frequency ranges $< 10^{11.5}$, $10^{11.5}$–10^{16}, and $> 10^{16}$ Hz, respectively, yielding 1327 sources suitable for further analysis. We discuss the properties of the discarded sources in §4.2.2.

For sources with unknown redshift ($\sim 16\%$ of the sample), we use the relationship between optical host galaxy magnitude and redshift of Sbarufatti et al. (2005) to estimate a value for these sources, taking the lower limit when exact host magnitudes were unavailable. All luminosities and frequencies were corrected to rest-frame values before spectral fitting; the global fits (rather than an assumed index) were then used to find k-corrected rest-frame quantities of interest.

2.2. *Jet Power*

Measuring the jet kinetic jet power of our blazars and radio galaxies allows us to see if the areas occupied by jets of similar power in the $\nu_{\rm peak} - {\rm L}_{\rm peak}$ plane can be understood simply as an orientation effect (as it would be anticipated in the original blazar sequence), or if additional considerations are needed. We note that for our purposes we need only classify sources into a few broad bins of jet power (as we show below, a width of one decade gives us a sufficient number of well populated jet power bins), and an extremely accurate estimation of the jet kinetic power is not needed.

Rawlings & Saunders (1991) estimated jet power by dividing the lobe energy content of radio galaxies by their age. The energy content was estimated through minimum energy arguments (*e.g.* Miley 1980) derived from measurements of the *low frequency radio emission* where the lobe emission is assumed to dominate over the jet, while the source age was estimated from spectral breaks in the lobe spectra through synchrotron aging arguments. Willott et al. (1999) revisited the issue of obtaining the jet power from the low frequency extended luminosity. They studied in detail the parameters that come into this relation, including the unknown energy content of the non-radiating particles and the time evolution of the lobe luminosity (see also Blundell et al. 1999) and presented a scaling relation which included a careful parametrization of the various uncertainties (see their Section 4.1, and Equation 11).

The actual normalization for this scaling between the jet kinetic power and the low frequency extended luminosity ($\rm L_{ext}$) came from a very different route. The dark cavities seen in (*e.g.*, Chandra) X-ray images are created by AGN jet activity and can be used to estimate the $p\Delta V$ work needed to inflate them. Importantly, this energy estimate does not depend on the minimum energy assumption and does not require knowledge of the amount of non-radiating matter in the lobes. The jet power $\rm L_{kin}$ is estimated by dividing the $p\Delta V$ work needed to expand the cavity by the cavity age found by estimating the lobe buoyancy time (Bîrzan et al. 2008; Cavagnolo et al. 2010).

While this method is limited to a small number of sources at present, the $\rm L_{kin} - L_{ext}$ relation covers almost six orders of magnitude in jet power, including both FR I and FR II sources. The slope of the scaling Cavagnolo et al. (2010) find is compatible within errors with that found by Willott et al. (1999) and requires a lobe energy content larger by at least a factor of 100 compared to that inferred by minimum energy arguments. The cavity work shows convincingly that $\rm L_{kin}$ and the ex-

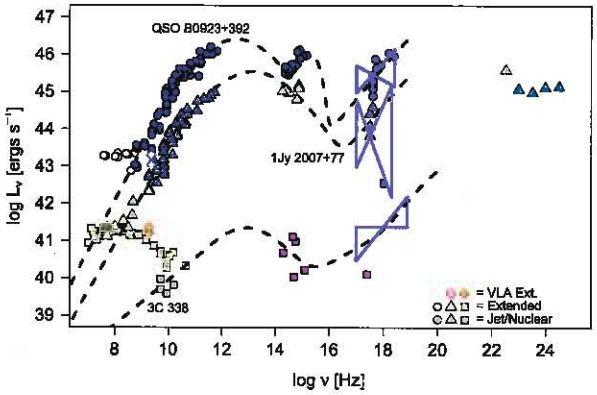

FIG. 1.— SEDs for three sources in which the extended radio emission is clearly visible as a steep component at low frequencies. The FSRQ QSO B0923+392 (top) has a very clear steep component at low frequencies, dominating up to $\sim 10^{9.5}$ Hz, and a prominent 'big blue bump' from the accretion disk, suggesting that it may be relatively misaligned compared with the *Fermi*-detected BL Lac 1Jy 2007+77 (middle), because they differ by ~ 2 decades in extended luminosity but only ~ 1 decade in beamed power. This latter source has a similar extended radio spectrum to the radio galaxy 3C 338 (bottom), however in the radio galaxy more of the extended emission is visible due to the nuclear emission being much less beamed. We also show estimates of the extended emission at 1.4 GHz as measured from VLA maps (diamonds), which generally agree with the spectral fits. The dashed curves are the best-fit of the blazar model described in the text and in Appendix A.

typical differences are less than 0.5 in log luminosity, with the best agreement found using a low-frequency index of $\alpha = 1.2$ for the extrapolation to 300 MHz.

The full SED for three sources is shown in Figure 1: the bright quasar QSO B0923+392 (top), the LSP BL Lac 1Jy 2007+77 (middle), and the FR I radio galaxy 3C 338 (bottom). In all cases, extended radio emission was detected in our two-component SD test – these points are shown in lighter colors of pink, green, and orange, respectively. (Estimates of the extended luminosity derived from VLA maps are also shown as diamonds). We note that while 1Jy 2007+77 and 3C 338 have similar extended luminosities at 300 MHz, the much greater core-dominance of the blazar is evident, and results in much less of the extended emission being visible. Also, while the quasar is evidently more powerful than the other two sources by two orders of magnitude in L_{300}, we see that it is likely more misaligned than 1Jy 2007+77, from the greater visibility of the steep component and the prominent accretion disk bump in the optical. This relatively bright source was also not a significant detection in the *Fermi*/LAT 1-year catalog, unlike 1Jy 2007+77. This could be explained if the gamma-ray emission is more beamed than that at lower frequencies.

2.2.2. *Connection Between Extended and Unbeamed Core Emission*

For the SD method, it is important to note that failure to find a two power-law solution for a source can just as easily be due to a lack of low-frequency data coverage as to the source emission being highly jet dominated down to low frequencies. The approximate frequency at which the beamed emission becomes dominant varies from 10^6 to 10^{13} Hz in our sample. In Figure 2 we plot the 'crossing' frequency $\nu_{\rm cross}$ of the fitted jet SED and steep component and the log core dominance R_{CE} (we define R_{CE} as the log of the ratio of core to extended luminosity at 1.4 GHz). The correlation is well-fit by a linear regression model (correlation coefficient $r = 0.87$). This correlation can arise from two coexisting causes: an intrinsic spread in unbeamed core power for a given extended luminosity and the effect of beaming. If the effect of the natural spread of core power dominates over the effects of beaming (as would be the case if beaming of the core emission is weak or absent), then we expect to see radio galaxies and blazars mixed along this correlation (this is because the range by which each particular source moves before being classified as a radio galaxy will be smaller than the initial intrinsic range that the aligned blazars populate). This is, however, not what we find, as shown in Figure 2. Instead, we observe a clear separation of radio galaxies and blazars which suggests that the effect of beaming dominates over the intrinsic spread and that the range of unbeamed core emission for a given extended luminosity be narrow.

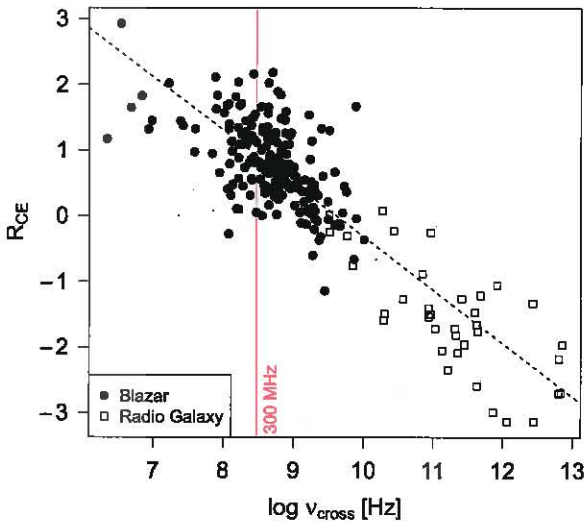

FIG. 2.— The crossing frequency, $\nu_{\rm cross}$ is the approximate frequency at which the SED becomes dominated by the beamed jet emission rather than the steep extended emission. Radio galaxies are shown as empty squares, and blazars as filled circles. As log core dominance (R_{CE}) increases due to beaming this crossing point moves to lower energies. Many sources will remain core-dominated to low frequencies, even to the limit of ground-based observations at ~ 10 MHz. The broken line shown is the linear correlation between the plotted variables ($r = 0.87$). The solid red line marks the 300 MHz frequency at which the extended emission is measured.

2.2.3. *Caveats*

Many of our sources which lack VLA imaging have observations down to very low frequencies ($30 - 200$ MHz), and show no signs of a steep component. It is impossible to tell if these sources are highly core-dominated to the lowest observed frequencies or if the lobe emission has a flat spectrum which is indistinguishable from the core emission. The latter scenario may be a concern for the very low power sources, as it is possible that the break frequency (*i.e.*, the point at which the lobe emission be-

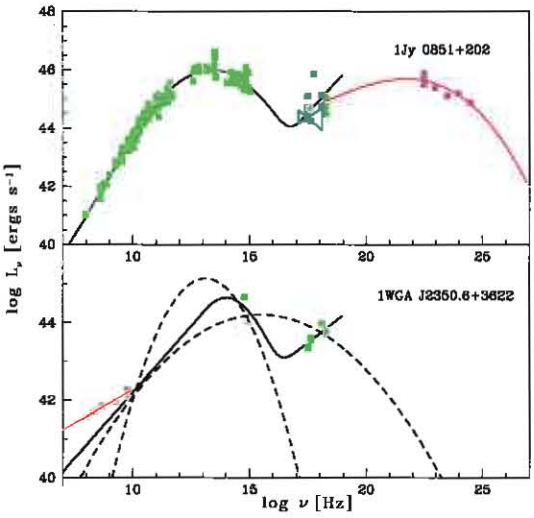

FIG. 3.— Examples of typical blazar SEDs in the master sample of flat-spectrum sources. Visual inspection of over 1300 SEDs was used to separate sources with unambiguous synchrotron peaks (top, 653 sources total) from those with under-sampled SEDs which might be consistent with several possible peak locations (bottom). The dark line is the best-fit model (described in Appendix A) for each case, while the dashed lines show other possible SED shapes consistent with the more sparsely-sampled SED.

comes steep) may increase with decreasing synchrotron power as Brunetti et al. (2003) found for hot spots in radio galaxies. For these sources it may be advisable to perform VLA map subtractions at multiple frequencies to confirm such a spectrum.

Finally, we must point out the risk in the common practice of assuming that flux below $\sim$ 300 MHz, taken without examination of the spectral characteristics, is actually from the extended isotropic component, rather than the core. This assumption would be clearly inappropriate for many of our sources, as shown by Figure 2, and could lead both to an overestimate of the jet power and an underestimate of the radio core dominance often used to infer the degree of mis-orientation of the source.

2.3. *Fitting the Synchrotron Spectrum*

For the 1327 blazars making the initial cut based on SED sampling, we utilized a phenomenological parametric model in order to estimate the synchrotron peak frequency and luminosity. The basic shape is parabolic, with a power-law extension to low frequencies and a rising power-law to simulate the beginning of the IC spectrum in the X-rays (Fossati et al. 1997). These components were free to vary within a reasonable range in shape or slope, respectively, and in relative normalization, for a total of 6 parameters. In sources where a big blue bump was suggested on visual inspection, this feature was added to the SED fit by adding a template accretion-disk spectrum (see Frank et al. 2002), adding one additional parameter for the bump peak luminosity (see Appendix A for a summary of the model).

To fit our model, we used a simulated annealing routine for the parameter search (Goffe et al. 1994), and an algorithm based on a combination of minimum square distance (in log L_ν) between model and data, with the added constraint of reasonable agreement with the X-ray spectral index where available, enforced by increasing the score of the fit by a function of the angle between the model and observed spectral slope.

We note that while simultaneous multi-wavelength observations give the best 'snapshot' view of an entire SED, such data is usually still biased by being limited to a single epoch, as the variability of these objects is well-known. The compilation of all available photometry, generally collected over a long time-frame, sampling many states of the SED, allows us to fit the model to the average SED of the source which may be more appropriate in a population context, in which extreme source states might confuse results.

2.4. *The TEX Sample of Blazars*

After fitting with the SED model, each source was subsequently examined by eye, in order to identify ambiguous cases where the formal best-fit model did not clearly represent the only reasonable SED fit. In many cases these removed sources had few data points in the critical region from IR to UV, lacked X-ray spectral indices, or had significant host galaxy contamination in the optical. A comparison of an acceptable and a rejected source with their best SED fits is shown in Figure 3. A total of 653 sources remained after this examination, in which we feel confident in the determination of the synchrotron peak to within one order of magnitude. (The rejected sources are discussed along with the other under-sampled blazars in §4.2.2). In total, 216 sources have robust estimates of ν_{peak}, L_{peak}, and L_{300}; this set comprises the TEX (trusted extended) sample. Of these, 129 have extended radio flux from spectral decomposition, 87 were added using only VLA map data, and 90 have both a spectral and VLA estimate. For the remaining 437 blazars comprising the UEX (unknown extended) sample, upper limits on L_{300} (and subsequently L_{kin}) were found by extrapolating from the luminosity at the lowest available frequency using $\alpha = 1.2$.

In Table 2 we list the sources which have a confirmed synchrotron peak and extended power measurement (TEX sample). In columns 1 – 5 we give the source name, position, optical type, and redshift. Estimated redshifts are noted by an asterisk in column 5. In columns 6 and 7 we give the best-fit synchrotron peak frequency and luminosity, respectively. In columns 8 and 9 we give L_{300} and the converted value of L_{kin}, respectively. In column 10 we note the method for the extended radio flux estimate: VLA, spectral decomposition (SD), or both. We note those sources (19 total) in which the spectral result is used instead of a VLA measurement by a dagger in that column. In column 11 we give the references for VLA data. All values are in the rest-frame of the source.

Because of the somewhat subjective requirement of an unambiguous synchrotron peak, the TEX sample does not contain all the sources in original list, and cannot be considered a complete sample. We focus most of our discussion on qualitative analysis and positive findings for our well-characterized sample. Relaxing the criteria for inclusion in the sample risks inaccurate measurements of the three principle quantities (ν_{peak}, L_{peak}, and L_{kin}) and could lead to incorrect conclusions. See §4.2 for a discussion of the selection effects of our master sample, the nature of the rejected sources, and the possible impact

TABLE 2
TEX Combined Blazar Source List

Name (1)	R.A. (J2000) (2)	Decl. (J2000) (3)	Opt.‡ (4)	z (5)	log ν_{peak} (Hz) (6)	log L_{peak} (ergs s^{-1}) (7)	log L_{300} (ergs s^{-1}) (8)	log L_{kin} (ergs s^{-1}) (9)	Method (10)	Ref. (11)
QSO B0003−06	00 06 13.89	−06 23 35.33	B	0.347	13.16	46.22	41.68	44.21	both	f,h
QSO B0016+73	00 19 45.73	+73 27 30.07	Q	1.781	13.26	47.65	42.61	44.74	both	f
QSO B0048−09	00 50 41.31	−09 29 05.21	B	0.200	13.43	44.97	41.20	43.93	both	b,d,f
4C 01.02	01 08 38.77	+01 35 00.27	Q	2.099	13.00	47.71	44.57	45.85	both	c,f,h
QSO B0109+224	01 12 05.82	+22 44 38.78	B	0.265	13.87	45.57	40.33	43.44	both	b,f,h
QSO B0118−272	01 20 31.66	−27 01 24.65	B	0.557	14.04	46.13	42.38	44.61	VLA	d
QSO B0133+47	01 36 58.58	+47 51 29.30	Q	0.859	13.34	46.63	41.93	44.35	VLA	f,h
QSO B0138−097	01 41 25.83	−09 28 43.67	B	0.733	13.49	46.22	42.41	44.62	VLA	d
4C 15.05	02 04 50.41	+15 14 11.04	Q	0.405	12.39	45.15	41.39	44.04	VLA	h
QSO B0212+73	02 17 30.82	+73 49 32.55	B	2.367	13.38	47.20	42.30	44.56	VLA	f,h
QSO B0215+015	02 17 48.95	+01 44 49.69	Q	1.715	13.72	47.71	43.52	45.26	VLA	b,f,h
QSO B0218+357	02 21 05.48	+35 56 13.70	Q	0.960	12.86	45.91	43.09	45.01	SD	
3C 66A	02 22 39.61	+43 02 07.80	B	0.444	13.98	46.34	42.85	44.87	both	b,e

Note. — Table 2 is published in its entirety in the electronic edition of the *Astrophysical Journal*. A portion is shown here for guidance regarding its form and content. Units of right ascension are hours, minutes, and seconds, and units of declination are degrees, arcminutes, and arcseconds.

* Redshift estimated from optical magnitude
† Spectral decomposition estimate of extended flux used instead of VLA estimate
‡ Optical Spectral Type. B = BL Lac, Q = FSRQ.
[b] Antonucci & Ulvestad (1985)
[c] Murphy et al. (1993)
[i] Cassaro et al. (1999)
[e] Landt & Bignall (2008)
[f] Kharb et al. (2010)
[g] Condon et al. (2002)
[h] Cooper et al. (2007)
[i] Caccianiga & Marchã (2004)

on our conclusions.

2.5. *Radio Galaxies*

As the jets isolated in radio galaxies are understood to be the less-beamed counterparts to blazars, one way to understand the relationship of the synchrotron peak and beaming in the envelope is to see where the synchrotron peak falls for these jets. In the context of the presumed blazar sequence, these 'hidden blazars' should indicate whether the sequence is preserved in misaligned jets. We take advantage of recent work to isolate the radio, IR, optical, and X-ray core emission from the jet in radio galaxies using high-resolution mapping to place as many radio galaxies as possible on the ν_{peak} - L_{peak} plane (Chiaberge et al. 1999; Capetti et al. 2000; Chiaberge et al. 2002; Capetti et al. 2002; Hardcastle et al. 2003; Trussoni et al. 2003; Balmaverde et al. 2006; Massaro et al. 2010; Buttiglione et al. 2011). We examine the 45 radio galaxies with extended radio flux measurements, and at least one radio, optical, and X-ray measurement of the nuclear emission available in the literature. The L_{300} for all radio galaxies was found from a parabolic fit[2] to the steep, low-frequency radio emission and subsequently converted to L_{kin} as in Equation 1. In all cases where available, VLA map-derived estimates at 1.4 GHz were in agreement with the spectral fits.

[2] For fitting the steep component in radio galaxies, a log-parabolic model is more appropriate than a power-law due to the much greater range of the spectrum visible, which usually has some curvature in νF_ν.

Fourteen radio galaxies are nearby, well-known sources, with core measurements at multiple frequencies which allow fitting of the synchrotron SED with the same parameterization as for the blazars. This set includes seven of the Fermi-detected *misaligned* AGN (Abdo et al. 2010b).

For the remaining 31 with sparser SED sampling, the synchrotron ν_{peak} was estimated using a non-parametric likelihood estimator. The joint distribution of R_{CE}, ν_{peak}, and the SED colors[3] α_{ro}, α_{ox} was calculated for all the sources in our TEX, UEX, and fitted radio galaxy samples. From this, a conditional, one-dimensional density on ν_{peak} can be found by supplying the other three observables. The value of the peak was taken as the maximum of this distribution, and we also report the 20% and 80% quartiles as the sampling error.

It is straightforward to estimate the peak luminosity from the radio luminosity at 5 GHz, with which it has a linear correlation (correlation coefficient r = 0.85). The linear fit (with 1-σ error) is

$$\log L_{peak} = 0.61\,(\pm 0.01)\ (\log L_{5GHz} - 43) + 45.68 \pm (0.02)\ [\mathrm{ergs\ s^{-1}}] \quad (2)$$

The 90% confidence interval, assuming a normal error distribution, corresponds to an uncertainty of $\Delta(\log L_{peak}) \simeq 0.8$.

The most likely peak frequency found by our statistical model for all radio galaxies is at or below 10^{14} Hz, with the exception of four FR II sources with moder-

[3] Spectral indices are defined at 1.4 GHz, 5000 Å, and 1 keV.

TABLE 3
RADIO GALAXIES

Name (1)	R.A. (J2000) (2)	Decl. (J2000) (3)	Morph.‡ (4)	z (5)	log ν_{peak} (Hz) (6)	log L_{peak} (ergs s^{-1}) (7)	log L_{300} (ergs s^{-1}) (8)	L_{kin} (ergs s^{-1}) (9)
3C 380†	18 29 31.77	+48 44 46.17	2	0.69	12.95	45.68	44.06	45.56
3C 17	00 38 20.52	-02 07 40.8	2	0.220	$13.05^{+0.30}_{-0.55}$	45.35	42.82	44.86
3C 18	00 40 50.35	+10 03 23.14	2	0.188	$12.83^{+0.32}_{-0.52}$	44.79	42.55	44.70
3C 29	00 57 34.92	-01 23 27.89	1	0.045	$12.94^{+0.39}_{-0.37}$	44.01	41.34	44.02
NGC 315	00 57 48.88	+30 21 08.81	1	0.016	$13.96^{+0.34}_{-0.65}$	43.94	39.78	43.13
3C 31	01 07 24.93	+32 24 45.20	1	0.017	$13.09^{+0.50}_{-0.41}$	43.53	40.79	43.70
3C 33.1	01 09 44.26	+73 11 57.17	2	0.181	$12.99^{+0.36}_{-0.25}$	44.30	42.42	44.63
3C 66B†	02 23 11.41	+42 59 31.38	1	0.02	13.36	42.09	40.73	43.67
3C 78†	03 08 26.22	+04 06 39.30	1	0.03	12.99	44.02	40.94	43.79
3C 83.1B	03 18 15.73	+41 51 27.38	1	0.025	$13.09^{+0.32}_{-0.62}$	43.40	40.93	43.78
3C 84†	03 19 48.16	+41 30 42.10	1	0.02	13.46	43.09	40.16	43.34
3C 111†	04 18 21.27	+38 01 35.80	2	0.05	13.28	43.29	41.41	44.05
3C 133	05 02 58.50	+25 16 24.0	2	0.278	$13.04^{+0.23}_{-0.22}$	45.08	42.98	44.95
3C 135	05 14 08.34	+00 56 31.63	2	0.127	$13.05^{+0.35}_{-0.36}$	43.79	42.04	44.41
3C 165	06 43 06.70	+23 19 00.3	2	0.296	$13.04^{+0.23}_{-1.04}$	44.33	42.80	44.84
3C 171	06 55 14.87	+54 08 59.4	2	0.238	$13.04^{+0.22}_{-0.22}$	43.89	42.73	44.81
3C 189†	07 58 28.10	+37 47 11.80	1	0.04	13.44	42.34	40.88	43.75
3C 264	11 45 05.00	+19 36 22.74	1	0.022	$12.60^{+0.52}_{-0.32}$	43.77	40.72	43.66
3C 270	12 19 23.21	+05 49 29.69	1	0.007	$13.16^{+0.31}_{-1.16}$	43.33	40.09	43.30
NGC 4278	12 20 06.82	+29 16 50.71	1	0.002	$12.96^{+0.39}_{-0.67}$	42.55	37.29	41.70
M 84†	12 25 03.74	+12 53 13.13	1	0.00	12.98	41.19	39.04	42.70
M 87†	12 30 49.42	+12 23 28.04	1	0.00	13.01	41.58	40.95	43.79
Cen A†	13 25 27.61	−43 01 08.80	1	0.00	12.72	41.47	40.21	43.37
3C 287.1	13 32 53.27	+02 00 45.79	2	0.216	$13.05^{+0.26}_{-1.05}$	45.21	42.38	44.61
3C 296†	14 16 52.92	+10 48 26.43	1	0.02	12.99	41.24	40.57	43.57
3C 300	14 23 01.00	+19 35 17.0	2	0.272	$12.73^{+0.40}_{-0.45}$	44.32	42.85	44.87
3C 317†	15 16 44.48	+07 01 18.00	1	0.03	12.83	42.95	41.34	44.01
3C 321	15 31 43.47	+24 04 18.93	2	0.096	$13.27^{+0.60}_{-0.48}$	44.19	41.86	44.31
B2 1553+24	15 56 03.87	+24 26 52.70	1	0.043	$13.11^{+0.31}_{-1.11}$	43.79	40.48	43.52
3C 338†	16 28 38.27	+39 33 04.97	1	0.03	13.12	41.44	41.18	43.92
NGC 6251†	16 32 31.96	+82 32 16.39	1	0.02	12.79	43.25	40.68	43.64
3C 346†	16 43 48.62	+17 15 48.97	1	0.16	13.46	43.49	42.25	44.53
Her A	16 51 08.14	+04 59 33.32	2	0.155	$13.04^{+0.22}_{-0.22}$	44.08	43.60	45.30
3C 349	16 59 32.00	+47 02 16.0	2	0.205	$12.94^{+0.25}_{-0.45}$	44.39	42.49	44.67
3C 388	18 44 02.41	+45 33 29.81	2	0.091	$13.03^{+0.46}_{-0.39}$	44.32	42.00	44.39
3C 442A	22 14 45.00	+13 50 47.66	1	0.026	$12.98^{+0.53}_{-0.65}$	42.74	40.77	43.69
3C 449	22 31 20.62	+39 21 29.81	1	0.017	$13.18^{+0.51}_{-0.57}$	43.27	40.17	43.35
B2 2236+35	22 38 29.46	+35 19 40.01	1	0.027	$13.04^{+0.23}_{-0.22}$	43.03	39.62	43.03
3C 452	22 45 48.78	+39 41 15.36	2	0.081	$13.02^{+0.23}_{-1.02}$	44.48	43.34	45.15
3C 460	23 21 28.50	+23 46 48.0	2	0.268	$13.04^{+0.24}_{-1.04}$	44.52	42.52	44.69
3C 465	23 38 29.39	+27 01 53.52	1	0.031	$13.07^{+0.38}_{-0.61}$	44.07	41.12	43.89

NOTE. — Units of right ascension are hours, minutes, and seconds, and units of declination are degrees, arcminutes, and arcseconds.

† Synchrotron peak estimated from blazar model fit to core fluxes

‡ Morphological Type. 1 = FR I, 2 = FR II.

ate jet powers ($L_{kin} \sim 10^{44.5}$ ergs s^{-1}) which display extreme X-ray luminosities. These sources include the broad-lined radio galaxies (BLRG) 3C 390.3 (which has been previously reported to have an LBL-like SED by Ghosh & Soundararajaperumal 1995) and 3C 332, as well as two lesser-studied narrow line radio galaxies, 3C 197.1 and 3C 184.1. The two BLRG have been detected with Swift and BeppoSAX in the hard X-ray (Grandi et al. 2006; Cusumano et al. 2010). All four sources were excluded from the final sample, as the X-ray is likely either thermal or from a strong IC component, and without knowledge of the synchrotron X-ray emission, any peak estimate would be practically arbitrary.

The final list of 41 radio galaxies is given in Table 3. Column descriptions are as in Table 2.

3. RESULTS

3.1. *The Blazar Envelope*

The TEX sample of 216 blazars, and the 41 radio galaxies are shown in the plane of L_{peak} versus ν_{peak} in

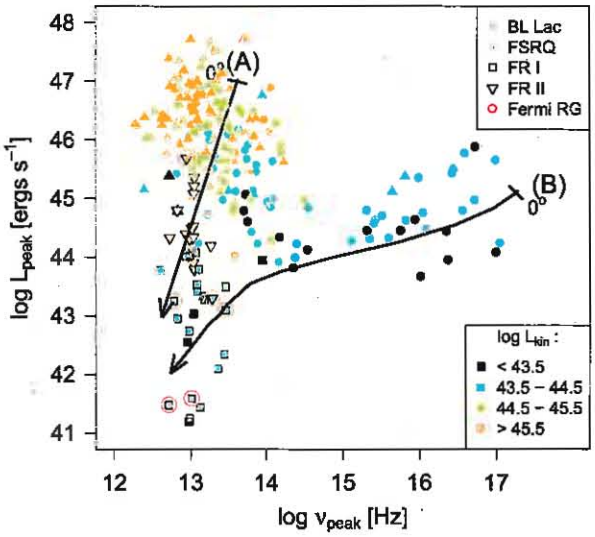

FIG. 4.— The blazar sequence, which originally showed an anti-correlation between synchrotron L_{peak} and ν_{peak} has been expanded into an 'envelope' with the addition of new observations and radio galaxies. BL Lacs are shown as filled circles, FSRQ as filled triangles, and radio galaxies as squares (FR I) and inverted triangles (FR II). Color indicates the jet kinetic power (L_{kin} in ergs s^{-1}), as estimated from extended radio flux measurements. Track (A) shows the path of a synchrotron peak for a single-component jet, and (B) for a decelerating jet of the type hypothesized to exist in FR I sources. The fully-aligned limit for each (0 degrees) is shown as marked, with the arrow direction indicating the movement of the model source as it is misaligned.

Figure 4. Blazars are represented as circles (BL Lacs) and triangles (FSRQ). The power of the source (L_{kin}) is shown by color in bins of one decade. Examining the location of blazars, there is an obvious lack of sources with both high jet powers *and* synchrotron peak frequencies above 10^{15} Hz, though a few of the ISP/HSP sources have quasar-like spectra. The population at low peak frequencies, alternately, is highly mixed in terms of kinetic power (with many low-power sources coincident with high-power sources), spectral type (with both BL Lac and quasar spectra present) and the spread of peak luminosities, which ranges from 10^{44} to $10^{47.5}$ ergs s^{-1}.

The 41 radio galaxies are shown in Figure 4 as squares (FR I) and inverted triangles (FR II). Those detected by *Fermi* (Abdo et al. 2010b) are circled in red. For our radio galaxy sample, we note that the jet power does not apparently exert much influence on their synchrotron peak frequency, and it appears that all radio galaxies in our sample exhibit jets with peaks below the optical-UV range in frequency. Further, no evidence is found for any conservation of a 'blazar sequence' within the radio galaxy jets shown here. If, as has been suggested, different emission regions in the less powerful jets dominate at different orientation angles (Chiaberge et al. 2000; Georganopoulos & Kazanas 2003; Ghisellini et al. 2005) it may simply be that the 'sequence' behavior (in which jet power regulates the synchrotron peak) pertains to the fast parts of the jet which are no longer visible in highly misaligned radio galaxies.

It becomes interesting to ask the question of what type of orientation tracks are expected on the L_{peak}-ν_{peak} plane if we assume that powerful sources do not decelerate, while weak sources require velocity gradients. The former assumption is supported by the fact that the Lorentz factors required to model the blazar SED of these sources ($\Gamma \sim 10 - 20$) are similar with those deduced from following VLBI superluminal components (e.g. Jorstad et al. 2001), while the latter (as we discussed in §1.2) is a result of our need to (*i*) explain the discrepancy between the high Lorentz factors required by the fast variability, pair production opacity, and SED modeling for the sub-pc scale jet and the lack of significantly superluminal motions at the VLBI scales and (*ii*) satisfy the unification between low power blazars and FR I radio galaxies.

Two tracks are shown in Figure 4. These illustrative tracks do not intend to simulate any particular source, and are shown to simply demonstrate how sources that start with the jet pointing toward us will appear as the jet orientation angle increases. The first, labeled (A), follows the misalignment of a powerful source assuming a single jet Lorentz factor $\Gamma = 15$. This track follows the expected 1:4 ratio of decreasing (log) frequency to (log) luminosity of the peak as the source is decreasingly beamed (see, *e.g.*, Lind & Blandford 1985). The second track, labeled (B), is for a weak source and shows the change in peak location for one possible model of a decelerating jet, as described in Georganopoulos & Kazanas (2003). In this particular example, the Lorentz factor of the flow decreases continuously from $\Gamma_{max} = 15$ to $\Gamma_{min} = 3$ in a distance of 5×10^{17} cm, and the emitted spectrum is calculated along the jet and integrated spatially. The track exhibits the qualitative characteristics (*e.g.*, more horizontal movement) not only consequent of the decelerating model, but of *any model* with velocity gradients in which the most energetic electrons are injected in the fast part of the flow, such as the spine-sheath model of Ghisellini et al. (2005). Such models, as can be seen in Figure 4, exhibit a shallow decrease of L_{peak} and a sharp decrease of ν_{peak} because the opening angle of the beaming cone is smaller for higher frequency emission; as the angle to the line of sight increases, progressively lower frequency emission is beamed away from the observer. Only for angles $\gtrsim 1/\Gamma_{min}$, do we expect the beaming track to start resembling that of a constant Lorentz factor flow and L_{peak} to start dropping faster with decreasing ν_{peak}. This model predicts that the low-power HSP blazars will follow a more horizontal path from the most beamed blazars to the misaligned radio galaxies. Interestingly, though each model originates in very different parts of the plane at low viewing angles, they coincide at higher orientation angles (*i.e.*, when seen as radio galaxy core emission).

3.2. *Radio Core Dominance*

In order to investigate the effect of viewing angle in populating the blazar envelope, it is necessary to have a way to measure or approximate the degree of misalignment in individual sources. The most readily available measure is the radio core dominance R_{CE}; typical values range from -3 (for the most off-axis radio galaxies) to ~ 3 (highly beamed quasars). As the extended emission is non-variable and unaffected by beaming, the dependence of R_{CE} on the orientation angle θ is directly due to the increased Doppler boosting factor at low angles.

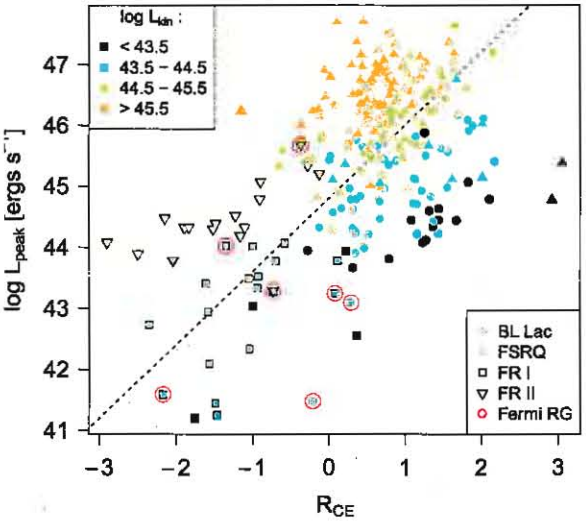

FIG. 5.— Core dominance (R_{CE}) versus synchrotron peak luminosity for BL Lacs, FSRQ, and radio galaxies in our sample. Color indicates the kinetic jet power (L_{kin} in ergs s^{-1}), as calculated from extended radio flux measurements, as in Figure 4. The dotted line has a slope equal to 1.2, the OLS bisector slope found for the whole sample. This slope is consistent with the expected relation between L_{peak} and L_R due to beaming effects.

The Doppler factor δ is given by

$$\delta = \frac{1}{\Gamma} \frac{1}{(1 - \beta cos\theta)}. \quad (3)$$

where Γ is the Lorentz factor of the jet and $\beta = v/c$. The Doppler-boosted luminosity for any part of the jet SED is a function of δ,

$$L = L_0 \delta^p \quad (4)$$

where L' is the unbeamed jet luminosity and $p = 2 + \alpha$ to $3 + \alpha$ depending on the geometry of the jet model, with α equal to the energy spectral index at the frequency of interest (see Urry & Padovani 1995). R_{CE} is thus a monotonically decreasing function of θ, though the exact shape is dependent on Γ, becoming steeper as θ increases. This does create a difficulty in comparing R_{CE} values directly for sources which may have very different bulk Γ values (such as, perhaps, very high and low power sources). However, if we assume that sources of the same jet power are similar in Γ, then we can compare at least these directly, and in general a source with a lower R_{CE} value will be more misaligned.

In order to investigate further how the sources of similar jet power are related in Figure 4, it would be helpful to add the core dominance. We thus examine how the core dominance changes with peak luminosity and frequency separately in Figures 5 and 6, still continuing to bin by the jet kinetic power as before. This choice is partly because it is practically difficult to add a 4th parameter in Figure 4, and also because, as suggested in Figure 5, the core dominance may have a different maximum (i.e., normalization), depending on the jet power, such that high-power sources have a lower maximum R_{CE} than that of the lowest power bin, making it difficult to compare sources at different powers directly. This can be understood if we make the assumption that unbeamed radio power scales from the overall jet power as $L'_R = \epsilon L_{kin}$ implying that jet radiative efficiency does not change much as the jet power increases. As we know $L_{kin} = \kappa L_{ext}^{\beta}$ (taking $\beta \sim 0.6$, see §2.2), this leads to the relation

$$\max R_{CE} = (1 - 1/\beta) \log L_{kin} + p \times \log(2\Gamma) + c_1 \quad (5)$$

where we have let $\delta_{max}=2\Gamma$, $c_1 = \log(\epsilon\kappa^{1/\beta})$, and $(1-1/\beta) \sim -2/3$. Assuming the last term is roughly constant, the maximum value of R_{CE} is thus *expected to decrease with increasing* L_{kin}, *even assuming reasonably different* Γ *values for high and low-power sources.* For example, taking p=2, and Γ=15 for a jet of $L_{kin} = 10^{46}$ predicts a max R_{CE} about 1.25 lower than for a jet with $L_{kin} = 10^{42}$ and Γ=3.

It is also expected that sources will separate by jet kinetic power in Figure 5, as following from the above equations, we have for the expected relation between R_{CE} and L_{peak}:

$$R_{CE} = \left(\frac{2 + \alpha_R}{3}\right) \log L_{peak} + \left(1 - \frac{1}{\beta}\right) \log L_{kin} + c_2 \quad (6)$$

It is clear that binning by L_{kin} will indeed induce the 'striping' in that figure through the second term, and that the slope in Figure 5 should be about 1.2 - 1.5 depending on the value of α_R (where we have assumed $p = 2 + \alpha$; see derivation in appendix B). However, scatter could be induced by the remaining term, $c_2 = \log(\epsilon\kappa^{1/\beta}) - (2+\alpha_R)\log L'_{peak}/3$ which is clearly determined by the relation between the unbeamed luminosity of a source at a given L_{kin}. If this quantity is not roughly constant with respect to L_{kin}, Figure 5 would be reduced to a multi-color scatter plot and the striping would be lost or degraded. It is also interesting to note that, like in Figure 2, there is a fairly uniform, sharp transition from blazars to radio galaxies in Figure 5. These arguments again suggest that beaming has a dominant effect on the observed (core) luminosity, rather than being due to a range of unbeamed core luminosities (L'_R, L'_{peak}) for a given L_{kin}.

A mild decrease in synchrotron peak frequency with increasing angle to the line of sight is expected in the simplest case of a jet dominated by a single Lorentz factor. The change in peak frequency as core dominance decreases is not significant for our sample of sources with L_{kin} greater than $10^{44.5}$ ergs s^{-1}, all of which have low synchrotron peak frequencies (these sources are therefore not shown in Figure 6). For low-power sources (less than $10^{44.5}$ ergs s^{-1}), however, there is a surprising pattern in the $R_{CE} - \nu_{peak}$ plane. As shown in Figure 6, there appears to be a clustering of sources with low peak frequencies and yet high core dominance, where R_{CE} reaches up to ~3, and another location at high peak frequencies where R_{CE} reaches ~1−1.5. Either locus could conceivably be connected via a misalignment track to the radio galaxies at lower left, but the source distribution suggests that there is not a smooth continuum between LSP and HSP sources. We expect a similar monotonic relationship between R_{CE} and ν_{peak} as was derived above for the peak luminosity, but this is clearly not consistent

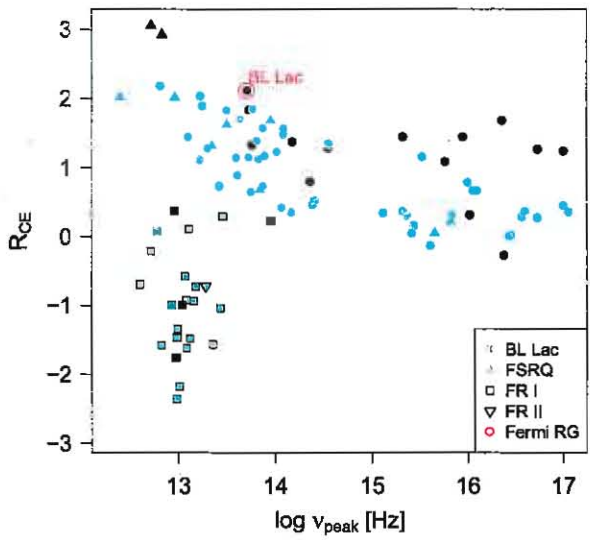

FIG. 6.— Core dominance (R_{CE}) versus the synchrotron peak frequency for all sources with L_{kin} below $10^{44.5}$ (L_{300} below $\sim 10^{42}$) ergs s^{-1}. While all low (kinetic) power radio galaxies have lower core dominance than blazars of similar power, there are apparently two locations of more aligned low-power blazars – one at low peak frequencies, with relatively higher R_{CE} values (up to 3), and another at high peak frequencies, with slightly lower R_{CE} values ($\sim$ 1–1.5). While nearly all sources at high peaks ($> 10^{15}$ Hz) are BL Lacs (*i.e.*, HBLs), the low-peaking aligned sources include a mixture of FSRQ and BL Lac spectral types. Color scale is the same as used in Figure 5.

with what is shown in Figure 6, at least if sources at low power consist of a single population.

In some cases the high core dominance values for the LSP sources at low powers could be due to systematic underestimation of L_{300} for these objects because of known problems with VLA measurements (incorrect modeling or use of an array configuration which might miss extended flux). However this would require nearly every single source to be over-estimated by an order of magnitude or more, and does not explain those LSP sources for which the steep spectrum is actually seen and matches the VLA estimate (such as BL Lac itself, noted in Figure 6).

4. DISCUSSION

4.1. *The Blazar Envelope*

Ghisellini et al. (1998) were able to reproduce the observed anti-correlations of the Fossati et al. (1998) blazar sequence using a simple one-zone leptonic jet model. They suggested that the increased radiative cooling of the electrons of high-power blazars lead to a particle energy distribution with a break at lower energies (leading to the lower peak frequency). In support of the scenario of a continuous spectral sequence, our results in Figure 4 clearly show a decreasing upper limit on L_{peak} as ν_{peak} increases. That sources near this limit are highly aligned, and those falling below are progressively misaligned is supported by the strong correlation between core dominance and peak luminosity shown in Figure 5 (which we note is much harder to appreciate without separating sources according to their radio galaxy or blazar classification and by their jet kinetic power). However, this simple scenario does not provide an explanation for the rather noticeable 'L' shape to the source distribution in Figure 4 or the wide range of synchrotron peak frequencies for sources of similar low jet powers. While the former might be the result of missing sources at intermediate peak frequencies, the latter is a positive finding that cannot be explained away as a selection effect.

4.1.1. *Jet Structures in the Envelope*

Ghisellini & Tavecchio (2008) revisited the theoretical blazar sequence, linking the power of the jet and the SED to two fundamental parameters of the accretion disk – the black hole mass and the accretion rate. Following Narayan et al. (1997) they assumed that sources with an accretion power (L_{acc}) lower than a critical value $L_{cr} = L_{Edd}\dot{m}_{cr}$ are radiatively inefficient accretors with weak or absent broad line region, while sources with $L_{acc} > L_{cr}$ are characterized by efficiently radiating accretion disks with strong big blue bumps and powerful broad line emission (where L_{Edd} is the Eddington luminosity and $\dot{m}_{cr} \sim 3 \times 10^{-3} - 10^{-2}$ a critical mass accretion rate in units of the Eddington accretion rate).

As discussed in §3 we see in our results the manifestation of two populations distinguished by typical jet structure. The first population have non-decelerating jets characterized by a single Lorentz factor. These sources do not contain a high-peaking synchrotron component and the increase in peak frequency as the jet is aligned is modest, leading to a concentration of blazars with synchrotron peak frequencies $\sim 10^{14}$ Hz even when fully aligned. The sources in this population include all of the more powerful blazars ($L_{kin} > 10^{44.5}$ ergs s^{-1}) and many sources at lower powers. We include the latter because of the high core dominance of many low-power, low-peaking blazars in Figure 6. The second population is only comprised of sources with L_{kin} below $\sim 10^{44.5}$ ergs s^{-1} and have complex, decelerating jets. These lower-power sources exhibit a high frequency-peaking synchrotron component when aligned.

The non-decelerating, low-peaking ('strong' jet) sources and decelerating, high-peaking ('weak' jet) sources form distinct populations which follow qualitatively different de-beaming paths in $L_{peak} - \nu_{peak}$ space, exampled by track (A) and (B) in Figure 4, respectively. The two population scenario explains the appearance of an L-shaped upper boundary as a natural consequence of the vertical and horizontal paths by sources through the $L_{peak} - \nu_{peak}$ plane. It also explains the appearance of Figure 6, as low power sources may be either strong or weak, producing considerable spread in possible ν_{peak} values as R_{CE} increases.

It is tempting to associate those weak sources (having $L_{kin} < 10^{44.5}$ erg s^{-1}) that we argue are characterized by velocity profiles (track B in Figure 4) with sources having $L_{acc} < L_{cr}$. If we assume that $L_{kin} \lesssim L_{acc}$ (e.g. Rawlings & Saunders 1991), this implies that the accretion power of these systems reaches at least up to $L_{acc} \sim 10^{44.5}$ erg s^{-1}, which for $\dot{m}_{cr} \sim 3 \times 10^{-3}$ corresponds to a black hole mass of $\sim 10^9$ $M_\odot$, in agreement with black hole mass estimates (e.g., Barth et al. 2002). Similarly, sources with $L_{kin} > 10^{44.5}$ erg s^{-1}, which are all of the powerful strong jet type (track A in Figure 4), must have $L_{acc} > L_{cr}$ or equivalently

$\dot{m} > \dot{m}_{cr} \sim 3 \times 10^{-3}$, assuming that black hole masses do not significantly exceed $\sim 10^9$ $M_\odot$.

In this framework, the low jet power sources ($L_{kin} < 10^{44.5}$ erg s^{-1}) that yet seem to have a strong jet may be explained as sources with relatively smaller black hole masses, such that although their jets are low power, the mass accretion rate required to sustain them is $\dot{m} > \dot{m}_{cr}$. Consider a jet with $L_{kin} = 10^{44}$ erg s^{-1} and black hole mass 10^8 $M_\odot$. From the above, it is clear that the accretion rate (in units of 10^{-3}) $\dot{m}_{-3} = 0.7$ $L_{kin,44}$ M_9^{-1} ~ 7, exceeds the critical value placing this relatively low power jet in the family of 'strong' jets.

4.1.2. *Optical Spectral Type and the Envelope*

While the original observational sequence of Fossati et al. (1998) implied a transition from quasars to line-less BL Lacs along a sequence from high to low bolometric luminosity, a firm distinction is not a necessary part of the theoretical scheme for a continuous blazar sequence. Ghisellini & Tavecchio (2008) explain the possibility of blue FSRQ, formed when the dissipation radius for the jet exceeds the radius of the broad line region, as well as lower-power FSRQ formed when an efficient accretion forms around a relatively small black hole, (the explanation we proposed in §4.1.1 is along the same lines). However, the traditional divide between BL Lacs and FSRQ, at an equivalent width of 5 Å may prove to be an essentially arbitrary one Ghisellini et al. (2010). As discussed in Georganopoulos & Marscher (1998), a line-less blazar may arise as a product of beamed emission out-shining the spectral lines, which would then emerge if the source were misaligned. A further complication arises when considering the spectral types of radio galaxies. High excitation radio galaxies (HERG) have prominent emission lines and presumably standard accretion disks accreting near the Eddington limit, while low excitation radio galaxies (LERG) have few or no lines and are likely radiatively inefficient. While most FR II are HERG and most FR I are LERG, there are known exceptions in both cases, including the nearby HERG FR I Cen A (Evans et al. 2004), other possible 'FR I quasars' (Blundell & Rawlings 2001; Heywood et al. 2007; Chiaberge et al. 2009), and an increasing population of LERG FR II at higher redshifts (up to $z \sim 0.5$, Garofalo et al. 2010).

An explanation is given by Garofalo et al. (2010) for the presence of these mixed-type AGN based on black hole spin – namely, that central black holes with high retrograde spins and efficient accretion will produce powerful HERG FR IIs, which slowly spin down to prograde-spinning, low efficiency FR Is. However, if the transition between spin state occurs significantly before or after the transition in accretion efficiency, mixed-state objects will occur. Interestingly, the spin-based unification scenario may explain the lack of an obvious continuum of blazar types, as in this scenario the transition objects (near zero spin) have much lower jet powers than rapidly spinning FR I or FR IIs, thus in our typical luminosity-dependent plots there will be a 'missing population' of transition objects, either showing up at much lower powers or missing due to selection effects.

Ultimately, it is not clear what role the ionizing continuum or line emitting regions has in influencing the jet type. Optical spectral type is therefore not a part of our suggested strong/weak classification, which relies instead on the source morphology, core-dominance, and location in the $\nu_{peak} - L_{peak}$ plane. Thus, many of the low-peaking sources with high core dominance (*i.e.*, strong jets) are BL Lacs, including BL Lac itself and all but one of the nine hot-spot BL Lacs found in the MOJAVE sample (Kharb et al. 2010). Similarly, several quasars appear at higher peak frequencies (*i.e.*, as weak jets) in the UEX sample.

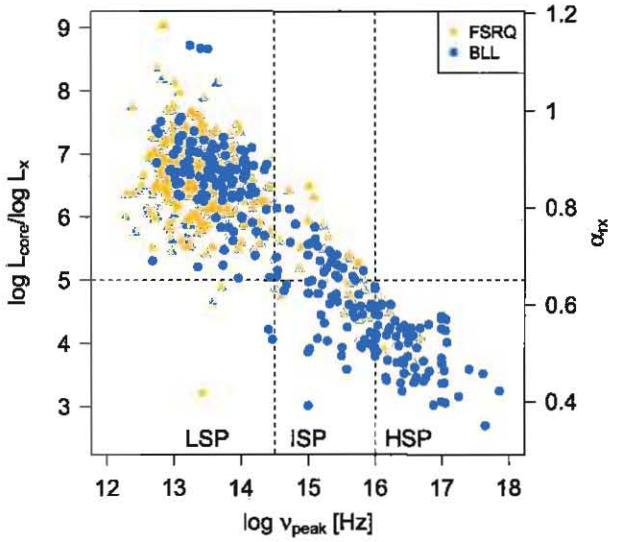

FIG. 7.— The ratio log (L_{core}/L_X) versus synchrotron peak frequency for all 653 sources with well-measured synchrotron peaks (equivalent α_{rx} is shown on the right scale, α_{rx} = log (L_{core}/L_X)/7.68). This ratio is often used to estimate the location of the synchrotron peak frequency when detailed SED information is lacking. Landt & Bignall (2008) use log (L_{core}/L_X) < 5 to indicate high synchrotron peak, however as shown, this ratio may only give a reliable upper limit to the frequency, and low log (L_{core}/L_X) values do not correspond exclusively to high synchrotron peaks.

Lastly, we comment on the possible presence of high-frequency-peaking FSRQ (HFSRQ) as claimed by several authors (Landt et al. 2006; Padovani et al. 2007; Landt et al. 2008). While the presence of quasars with low bolometric luminosities and high peaks (essentially having SEDs typical of HSP BL lacs) are consistent with expectations based on the updated theoretical sequence (Ghisellini & Tavecchio 2008), many of the objects discussed do have higher jet kinetic powers typical of FR IIs. However, using low core radio to X-ray flux (log L_{core}/log L_X < 5) or high optical to X-ray ratio (α_{ox}) is not a reliable way to find sources with high ν_{peak}. To illustrate this, in Figure 7 we plot log (L_{core}/L_X), measured at 5 GHz and 1 keV, against the known peak from our SED fits (based on much more extensive data than a two-point spectral index) for the 653 sources in our TEX+UEX sample. While a few quasars exist in the HSP range > 10^{16} Hz, these sources appear otherwise very similar to HSP BL Lacs in their SEDs. Further, many sources below the log (L_{core}/L_X) < 5 limit clearly have low peak values, often with a hard X-ray spectrum indicating a non-synchrotron origin. So far no unambiguous evidence of any blazar with a high peak frequency *and high luminosity* (above the typical HSP zone) has

TABLE 4
OVERVIEW OF STRONG AND WEAK JET CLASSES

	Strong	Weak
Definition	More powerful, single-component jet (single characteristic Γ), remains relativistic on large scales	Lower-power jet with faster deceleration, multiple emitting regions (multiple Γ)
Optical Type	mostly FSRQ	mostly BL Lacs
Synchrotron Peak	All high-power LSP, some low-power LSP	All ISP, HSP, some low-power LSP
Typical L_{300}	$10^{40} - 10^{45}$ ergs s^{-1}	$10^{38} - 10^{42}$ ergs s^{-1}
Typical L_{kin}	$10^{43.5} - 10^{46}$ ergs s^{-1}	$10^{42} - 10^{44.5}$ ergs s^{-1}
Radio Morphology	FR II; Collimated jets, hot spots, edge-brightened	FR I; Less collimated, edge-darkened, no hot spots
Accretion Type	Efficient, likely standard disk	Inefficient, highly sub-Eddington

been found (see Maraschi et al. 2008; Landt et al. 2008).

4.1.3. *Intermediate and Low-peaking Blazars*

According to the proposed two-population scenario, all ISP and HSP sources belong to the weak jet parent sample along with FR I radio galaxies. As blazars, they move from a population of HSP to ISP and finally LSP sources as they are misaligned. Contrary to the interpretation of a continuous sequence (Fossati et al. 1998), then, ISP blazars should have lower core dominance, lower overall luminosities, lower Doppler factors, and yet similar L_{kin} when compared with HSP sources. However, it is difficult to rule out a missing population of intermediate sources which may fill in the gap between low and high peaks in Figure 6 or in the center of Figure 4. These less populated regions are not due to the flux-limited selections of the original master sample (see below). If these sources are in the master sample, the SED sampling would have to be much lower, and for such relatively bright objects, this seems unlikely.

Weak jet sources at even greater angles to the line of sight should appear as LSP blazars, though they may not be recognizable as such (but rather as radio galaxies). Regardless, these should be distinguishable from strong jet LSP sources based on core dominance, morphology, extended radio power, and polarization signatures. However without detailed VLBI and VLA studies to measure these attributes, confusion among the two LSP populations is likely to occur. From our hypothesis that R_{CE} must decrease with peak frequency for weak-jet sources, we expect most of the low-power LSP blazars shown in Figure 6 to belong to the parent sample of strong jet sources, along with FR II radio galaxies. This connection is suggested by the equal or higher core dominance of most of these sources compared with the HSP blazars in the same L_{kin} range. It is also supported by the detailed observations we do have from VLBI studies of some of our objects, such as the nine LSP BL Lacs in the MOJAVE sample with hotspots similar to those typically seen in high-powered quasars and associated with FR II morphology (Kharb et al. 2010). The MOJAVE blazars (almost entirely LSP sources) were also found to have an intrinsic, unbeamed luminosity function consistent with that of FR II radio galaxies, whether BL Lacs were included or not (Cara & Lister 2008).

We summarize the strong and weak jet characteristics as suggested by the current work in Table 4.

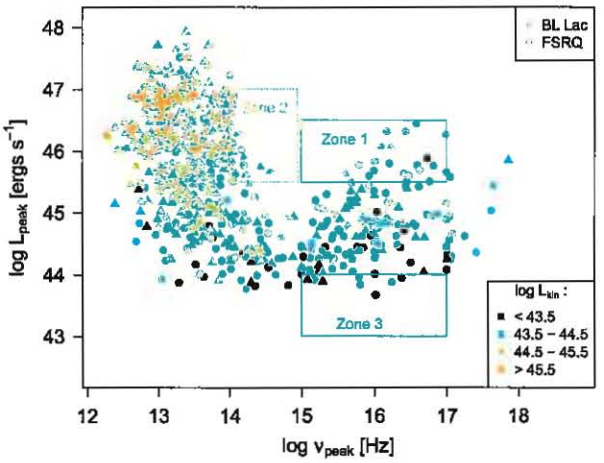

FIG. 8.— The blazar envelope for the UEX sample of 437 sources with only upper limits on L_{kin}. Upper limits were found by extrapolating from the lowest frequency observation of core flux using a spectral index $\alpha = 1.2$. The same color scale is used as in Figure 4. We clearly see a similar 'L' shape as is suggested in the figure for TEX sources. Also shown are the three zones discussed in §4.2.

4.2. *Examining the Sample Bias*

Our effort is concerned with those sources which can be placed on the $\nu_{peak} - L_{peak}$ plane with confidence, which is primarily a function of SED sampling. It is important to examine both the selection of the entire sample and the nature of the discarded objects for evidence of any bias which might produce the current findings.

One possible selection bias is a 'windowing' effect due to the low frequency radio measurements required to isolate the core and extended components. On one side, very core-dominated sources are likely to be missed when using only the spectral decomposition method, as these might not exhibit a steep spectrum except below very low frequencies (10 – 100 MHz) which are not frequently observed (and thus fail the two-component test). On the other side, a very de-beamed source may not qualify as a flat-spectrum source if the ν_{cross} is much above typical sample definition frequencies of a few GHz. The combined effect could in principle lead to the selection of sources for which the core and extended fluxes are

by constraint rather similar. The inclusion of VLA map data, which allows us to find extended flux densities even in very core-dominated sources, should mitigate the first issue. As to the second, as we show in Figure 2, most blazars are core dominated above the crucial window of a few GHz, and we detect a few above this limit. Between the blazars and radio galaxies in this figure there is no large gap indicating a missing population, and we do not find any reasons to suspect that the windowing effect is a problem for the results of this paper.

4.2.1. *Upper Limits*

The over 400 sources in the UEX sample are shown in Figure 8, with the color corresponding to the upper limit of the jet kinetic power. The overall shape of the envelope appears qualitatively similar to Figure 4.

We tested areas of the $\nu_{\rm peak} - {\rm L}_{\rm peak}$ plane using simulations to check how the sensitivity to sources in the plane is affected by our overall combined sample selection (*i.e.*, the combined selection of the samples in Table 1). We moved ~100 template SEDs drawn from our database to various peak locations in each zone shown in Figure 8 and simulated cuts using the flux limits of our individual samples. In zones 1 and 2, we did not find any difficulty detecting the simulated sources out to a reasonable redshift (z ~2). In zone 3, however, our sample would likely only include sources out to $z \sim 0.2$, which is not much less than the typical redshift of the HSP sources just above this region ($z \sim 0.25$). We conclude that the particular lack of ISP sources with L_{peak} intermediate between LSP and HSP sources is not due to the *initial* selection of our sample. For at least zones 1 and 2, which would contain very bright sources, it is unlikely that a large number of sources would exist there, but lack the SED sampling necessary to make the more subjective cuts leading to our final sample.

4.2.2. *Remaining Sample*

We now examine the sources which we were unable to include due to inadequate SED sampling (typically fewer than ~ 10 SED data points). Examination of the colors (radio-optical and optical-X-ray indices) for these sources indicates that they have values consistent with the well-characterized sample of ~ 600 TEX+UEX sources. Unsurprisingly, those with X-ray detections mostly populated the 'HSP zone' of the $\alpha_{ro} - \alpha_{ox}$ plane, indicating that a large population of the excluded sources are likely higher redshift HSPs and ISPs.

The optical and X-ray luminosity distributions for the excluded sample as a whole are indistinguishable (by KS test) from the TEX+UEX sample. In all three bands (and in particular the radio), those sources detected in the X-rays tended to have much lower luminosities, and are therefore unlikely to populate the so-called 'forbidden zone' of high synchrotron peak luminosity and frequency. Those not detected in X-rays had a distribution of $\alpha_{\rm ro}$ typical of LSP sources, but actually tended to have higher luminosities than our TEX+UEX sample. However, non-detection in X-rays and higher redshifts in general probably explains their absence in the TEX+UEX sample. Overall, none of the sources excluded from the TEX+UEX sub-sample appear to be substantially different from those in it; however, only additional multi-frequency observations of these sources can confirm this.

5. SUMMARY AND CONCLUSIONS

In this work we have analyzed the multi-frequency spectrum of several hundred blazars in order to accurately measure the synchrotron peak frequency and luminosity, and performed spectral analysis of the low-frequency emission in order to estimate the intrinsic jet power by a scaling of the 300 MHz extended radio power. The connection of blazars and radio galaxies in the same plane amounts to an extension of the original blazar sequence to a blazar envelope, in which highly aligned blazars form an upper limit in the $\nu_{\rm peak} - {\rm L}_{\rm peak}$ plane, while radio galaxies populate the lower left. We find that the jet power does not absolutely determine the $\nu_{\rm peak}$ of a maximally-beamed source. Instead, there seems to a break-down at low kinetic jet power, such that these jets are capable of having either low or high synchrotron peaks when aligned with the line of sight.

Our results suggest a shift away from the continuous blazar sequence interpretation, but confirmation waits for ever more data. We summarize the most important points here:

- Among our sample of over 600 blazars with well-sampled blazar SEDs, none with high peak frequencies and high luminosities are found. This void may be explained by the original arguments advanced by Ghisellini et al. (1998), that higher external radiation fields in high-power sources lead to greater cooling and thus lower break/peak energies.

- However, it is not clear that there is a continuum of SED types with jet power. The source power alone does not appear to determine the placement of a source along the aligned sequence. Instead, we suggest that radio-loud AGN can be divided into two populations: low-synchrotron-peaking sources without significant velocity gradients or deceleration (strong jets) and high-synchrotron-peaking sources which do have such structure (weak jets). The attributes of these samples are summarized in Table 4.

- It appears that below a certain jet power, sources can either have strong or weak jets, suggesting another parameter besides kinetic power is responsible for the jet structure. As in Ghisellini & Tavecchio (2008), we suggest that this parameter is the accretion rate $\dot{m}$ in Eddington units with the two families separated at $\dot{m} = \dot{m}_{cr} \sim 3 \times 10^{-3} - 10^{-2}$, with sources having $\dot{m} < \dot{m}_{cr}$ exhibiting radiatively inefficient accretion (Narayan et al. 1997).

- A key prediction of the two-population scenario is that ISP sources primarily consist of misaligned HSP objects, as suggested by their slightly lower L_{peak} values and similar L_{kin} to HSPs. Observations of ISP sources with synchrotron peak values and core dominance values between those typical of the LSP and HSP sources (currently missing) would support a continuous sequence interpretation instead.

- Observations of highly core-dominated, low-peaking BL Lacs (such as BL Lac itself), including

several BL Lacs exhibiting FR II-like morphology, leads us to speculate that these sources belong to the strong-jet parent population, along with FR II radio galaxies. Likewise, some ISP and HSP sources with quasar-like spectra in our sample belong to the weak population. Thus the spectral types associated with strong and weak jets are mixed.

- The low peak frequencies seen in our FR I radio galaxies supports the interpretation of a horizontal movement in the $\nu_{\rm peak} - {\rm L}_{\rm peak}$ plane for weak sources which supports a model with velocity profiles in the jet and leads to our two-population scheme. Observations of high synchrotron peaks in radio galaxies would be very difficult to explain under this scenario.

The authors wish to thank the anonymous referee for helpful comments, and Katherine Blundell for a discussion which lead to the improvement of this manuscript. This research has made use of the SIMBAD database, operated at CDS, Strasbourg, France (http://simbad.u-strasbg.fr/simbad/), and the NASA/IPAC Extragalactic Database (NED) which is operated by the Jet Propulsion Laboratory, California Institute of Technology, under contract with the National Aeronautics and Space Administration (http://nedwww.ipac.caltech.edu/). We utilized package *np* (Hayfield & Racine 2008) in the *R* language and environment for statistical computing (R Development Core Team 2010). GF acknowledges support from NASA grants NNG05GJ10G, NNX06AE92G, and NNX09AR04G, as well as SAO grants GO3-4147X and G05-6115X. MG acknowledges support from the NASA ATFP grant NNX08AG77G and NASA FERMI grant NNH08ZDA001N. The MOJAVE project is supported under National Science Foundation grant 0807860-AST.

APPENDIX

A. PHENOMENOLOGICAL BLAZAR SED MODEL

The model was adapted from Fossati et al. (1997) and used to fit the average blazar SED with seven parameters, six of which were free to vary and which were optimized using an SA routine.
Parameters:

$$\begin{array}{ll} L_R = & 32-46 \\ \tau \equiv & 1000 \\ x_{\rm j} = & 1-4 \\ \kappa_{\rm rx} = & 3-9 \\ \alpha_x = & -0.4-0.8 \\ x_{\rm peak} = & 10-20 \\ \beta = & 0.6-2.0 \end{array}$$

To build the SED, the following equations were combined, where $\vec{x} = \log(\vec{\nu})$. Vector quantities are noted with arrows for clarity, and luminosities are in log.

$$\sigma = \sqrt{\frac{2\,x_{\rm j}}{\beta}} \tag{A1}$$

$$L_{\rm peak} = \beta\,(x_{\rm peak} - x_{\rm j} - 9.698) + L_{\rm R} + \left(\frac{1}{2}\,\beta\,x_{\rm j}\right) \tag{A2}$$

$$\vec{c}_{\rm damp} = \begin{cases} 1 & \text{when } \vec{x} < x_{\rm peak} \\ 2 - 10^{\frac{\vec{x}-x_{\rm peak}}{\tau}} & \text{else} \end{cases} \tag{A3}$$

$$\vec{L}_{\rm synch} = \begin{cases} \beta\,(\vec{x} - 9.698) + L_{\rm R} & \text{when } \vec{x} < (x_{\rm peak} - x_{\rm j}) \\ \left[L_{\rm peak} - \left(\frac{\vec{x}-x_{\rm peak}}{\sigma}\right)^2\right] \vec{c}_{\rm damp} & \text{else} \end{cases} \tag{A4}$$

$$\vec{L}_{\rm IC} = L_R - \kappa_{\rm rx} + 7.685 + (1-\alpha_x)\,(\vec{x} - 17.383) \tag{A5}$$

Finally, we have the complete SED:

$$\vec{L} = \log\left[10^{\vec{L}_{\rm synch}} + 10^{\vec{L}_{\rm IC}}\right] \tag{A6}$$

B. RADIO CORE DOMINANCE

Equation 6 can be derived starting from the definition of log core dominance ratio R_{CE}:

$$R_{CE} = \log\left(\frac{L_R}{L_{ext}}\right) \tag{B1}$$

where L_{ext} and L_R are the luminosities of the extended and core components taken at the same frequency, and the beaming equations for the luminosity for the radio and synchrotron peak frequency are simply:

$$L_R = L'_R \delta_R^{p_R} \tag{B2}$$

$$L_{peak} = L'_{peak} \delta_{peak}^{p_{peak}} \tag{B3}$$

where δ_R and δ_{peak} are the Doppler factors for the jet regions dominating the emission at those frequencies, and the exponents take values $p = 2+\alpha$ or $3+\alpha$, depending on the jet model, and with α the spectral indices in the band of interest. By taking advantage of the relationship $L_{kin} = \kappa L_{ext}^{\beta}$ (see §3.2) we can rewrite it as:

$$R_{CE} = \log\left(\frac{L'_R \delta_R^{p_R}}{\left(\frac{L_{kin}}{\epsilon}\right)^{1/\beta}}\right) \tag{B4}$$

If we assume that $L'_R = \epsilon L_{kin}$ (see §3.2), and that the bulk Lorentz factors Γ for the radio and the peak emission are the same, such that $\delta_R = \delta_{peak}$, using B3, we obtain:

$$R_{CE} = \log\left(\epsilon L_{kin}\left(\frac{L_{peak}}{L'_{peak}}\right)^{\frac{p_R}{p_{peak}}}\right) - \log\left(\frac{L_{kin}}{\kappa}\right)^{1/\beta} \tag{B5}$$

Letting $p_R = 2 + \alpha_R$ and $p_{peak} = 2 + \alpha_{peak} = 3$, we have equation 6:

$$R_{CE} = \left(\frac{2+\alpha_R}{3}\right)\log L_{peak} + \left(1 - \frac{1}{\beta}\right)\log L_{kin} + c_2 \tag{B6}$$

$$c_2 = \log(\epsilon\kappa^{1/\beta}) - \left(\frac{2+\alpha_R}{3}\right)\log L'_{peak} \tag{B7}$$

REFERENCES

Abdo, A. A., et al. 2010a, ApJS, 188, 405
—. 2010b, ApJ, 720, 912
—. 2010c, ApJ, 716, 30
Aharonian, F., et al. 2007, ApJ, 664, L71
Antonucci, R. R. J., & Ulvestad, J. S. 1985, ApJ, 294, 158
Balmaverde, B., Capetti, A., & Grandi, P. 2006, A&A, 451, 35
Barth, A. J., Ho, L. C., & Sargent, W. L. W. 2002, ApJ, 566, L13
Beckmann, V., Engels, D., Bade, N., & Wucknitz, O. 2003, A&A, 401, 927
Bîrzan, L., McNamara, B. R., Nulsen, P. E. J., Carilli, C. L., & Wise, M. W. 2008, ApJ, 686, 859
Blundell, K. M., & Rawlings, S. 2001, ApJ, 562, L5
Blundell, K. M., Rawlings, S., & Willott, C. J. 1999, AJ, 117, 677
Böttcher, M. 2007, Ap&SS, 309, 95
Brunetti, G., Mack, K.-H., Prieto, M. A., & Varano, S. 2003, MNRAS, 345, L40
Buttiglione, S., Capetti, A., Celotti, A., Axon, D. J., Chiaberge, M., Macchetto, F. D., & Sparks, W. B. 2011, A&A, 525, A28+
Caccianiga, A., Maccacaro, T., Wolter, A., della Ceca, R., & Gioia, I. M. 1999, ApJ, 513, 51
Caccianiga, A., Marchã, M. J., Antón, S., Mack, K.-H., & Neeser, M. J. 2002, MNRAS, 329, 877
Caccianiga, A., & Marchã, M. J. M. 2004, MNRAS, 348, 937
Capetti, A., Celotti, A., Chiaberge, M., de Ruiter, H. R., Fanti, R., Morganti, R., & Parma, P. 2002, A&A, 383, 104
Capetti, A., Trussoni, E., Celotti, A., Feretti, L., & Chiaberge, M. 2000, MNRAS, 318, 493
Cara, M., & Lister, M. L. 2008, ApJ, 674, 111
Cassaro, P., Stanghellini, C., Bondi, M., Dallacasa, D., della Ceca, R., & Zappalà, R. A. 1999, A&AS, 139, 601
Cavagnolo, K. W., McNamara, B. R., Nulsen, P. E. J., Carilli, C. L., Jones, C., & Bîrzan, L. 2010, ApJ, 720, 1066
Chiaberge, M., Capetti, A., & Celotti, A. 1999, A&A, 349, 77
—. 2002, A&A, 394, 791
Chiaberge, M., Celotti, A., Capetti, A., & Ghisellini, G. 2000, A&A, 358, 104
Chiaberge, M., Tremblay, G., Capetti, A., Macchetto, F. D., Tozzi, P., & Sparks, W. B. 2009, ApJ, 696, 1103
Cohen, M. H., Lister, M. L., Homan, D. C., Kadler, M., Kellermann, K. I., Kovalev, Y. Y., & Vermeulen, R. C. 2007, ApJ, 658, 232
Condon, J. J., Cotton, W. D., & Broderick, J. J. 2002, AJ, 124, 675
Cooper, N. J., Lister, M. L., & Kochanczyk, M. D. 2007, ApJS, 171, 376
Corbett, E. A., Robinson, A., Axon, D. J., & Hough, J. H. 2000, MNRAS, 311, 485
Cusumano, G., et al. 2010, A&A, 510, A48+
Dondi, L., & Ghisellini, G. 1995, MNRAS, 273, 583
Edwards, P. G., & Piner, B. G. 2002, ApJ, 579, L67
Evans, D. A., Kraft, R. P., Worrall, D. M., Hardcastle, M. J., Jones, C., Forman, W. R., & Murray, S. S. 2004, ApJ, 612, 786
Fanaroff, B. L., & Riley, J. M. 1974, MNRAS, 167, 31P
Fossati, G., Celotti, A., Ghisellini, G., & Maraschi, L. 1997, MNRAS, 289, 136
Fossati, G., Maraschi, L., Celotti, A., Comastri, A., & Ghisellini, G. 1998, MNRAS, 299, 433
Frank, J., King, A., & Raine, D. J. 2002, Accretion Power in Astrophysics: Third Edition, ed. Frank, J., King, A., & Raine, D. J.
Garofalo, D., Evans, D. A., & Sambruna, R. M. 2010, MNRAS, 406, 975
Georganopoulos, M., & Kazanas, D. 2003, ApJ, 594, L27
Georganopoulos, M., & Marscher, A. P. 1998, ApJ, 506, 621

Ghisellini, G., Celotti, A., Fossati, G., Maraschi, L., & Comastri, A. 1998, MNRAS, 301, 451
Ghisellini, G., & Tavecchio, F. 2008, MNRAS, 387, 1669
Ghisellini, G., Tavecchio, F., Bodo, G., & Celotti, A. 2009, MNRAS, 393, L16
Ghisellini, G., Tavecchio, F., & Chiaberge, M. 2005, A&A, 432, 401
Ghisellini, G., Tavecchio, F., Foschini, L., & Ghirlanda, G. 2010, ArXiv e-prints
Ghosh, K. K., & Soundararajaperumal, S. 1995, ApJS, 100, 37
Giannios, D., Uzdensky, D. A., & Begelman, M. C. 2009, MNRAS, 395, L29
Giommi, P., Menna, M. T., & Padovani, P. 1999, MNRAS, 310, 465
Giommi, P., Piranomonte, S., Perri, M., & Padovani, P. 2005, A&A, 434, 385
Giroletti, M., et al. 2004, ApJ, 600, 127
Goffe, W., Ferrier, G., & Rogers, J. 1994, Journal of Econometrics, 60, 65
Grandi, P., Malaguti, G., & Fiocchi, M. 2006, ApJ, 642, 113
Hardcastle, M. J., Worrall, D. M., Birkinshaw, M., & Canosa, C. M. 2003, MNRAS, 338, 176
Hayfield, T., & Racine, J. S. 2008, Journal of Statistical Software, 27
Healey, S. E., et al. 2008, ApJS, 175, 97
Heywood, I., Blundell, K. M., & Rawlings, S. 2007, MNRAS, 381, 1093
Hine, R. G., & Longair, M. S. 1979, MNRAS, 188, 111
Hook, I. M., Shaver, P. A., Jackson, C. A., Wall, J. V., & Kellermann, K. I. 2003, A&A, 399, 469
Jackson, C. A., Wall, J. V., Shaver, P. A., Kellermann, K. I., Hook, I. M., & Hawkins, M. R. S. 2002, A&A, 386, 97
Jorstad, S. G., Marscher, A. P., Mattox, J. R., Wehrle, A. E., Bloom, S. D., & Yurchenko, A. V. 2001, ApJS, 134, 181
Kharb, P., Lister, M. L., & Cooper, N. J. 2010, ApJ, 710, 764
Landt, H., & Bignall, H. E. 2008, MNRAS, 391, 967
Landt, H., Padovani, P., Giommi, P., Perri, M., & Cheung, C. C. 2008, ApJ, 676, 87
Landt, H., Padovani, P., Perlman, E. S., Giommi, P., Bignall, H., & Tzioumis, A. 2001, MNRAS, 323, 757
Landt, H., Perlman, E. S., & Padovani, P. 2006, ApJ, 637, 183
Laurent-Muehleisen, S. A., Kollgaard, R. I., Feigelson, E. D., Brinkmann, W., & Siebert, J. 1999, ApJ, 525, 127
Lind, K. R., & Blandford, R. D. 1985, ApJ, 295, 358
Lister, M. L., et al. 2009, AJ, 138, 1874
Londish, D., et al. 2002, MNRAS, 334, 941
—. 2007, MNRAS, 374, 556
Maraschi, L., Foschini, L., Ghisellini, G., Tavecchio, F., & Sambruna, R. M. 2008, MNRAS, 391, 1981
Marchã, M. J., Caccianiga, A., Browne, I. W. A., & Jackson, N. 2001, MNRAS, 326, 1455
Massaro, F., et al. 2010, ApJ, 714, 589
Miley, G. 1980, ARA&A, 18, 165
Morris, S. L., Stocke, J. T., Gioia, I. M., Schild, R. E., Wolter, A., Maccacaro, T., & della Ceca, R. 1991, ApJ, 380, 49
Mukherjee, R., et al. 1997, ApJ, 490, 116
Murphy, D. W., Browne, I. W. A., & Perley, R. A. 1993, MNRAS, 264, 298
Narayan, R., Garcia, M. R., & McClintock, J. E. 1997, ApJ, 478, L79+
Padovani, P., Giommi, P., Landt, H., & Perlman, E. S. 2007, ApJ, 662, 182
Perlman, E. S., Padovani, P., Giommi, P., Sambruna, R., Jones, L. R., Tzioumis, A., & Reynolds, J. 1998, AJ, 115, 1253
Perlman, E. S., et al. 1996, ApJS, 104, 251
Piner, B. G., Jones, D. L., & Wehrle, A. E. 2001, AJ, 122, 2954
Piner, B. G., Pant, N., & Edwards, P. G. 2008, ApJ, 678, 64
—. 2010, ApJ, 723, 1150
Piranomonte, S., Perri, M., Giommi, P., Landt, H., & Padovani, P. 2007, A&A, 470, 787
Plotkin, R. M., Anderson, S. F., Hall, P. B., Margon, B., Voges, W., Schneider, D. P., Stinson, G., & York, D. G. 2008, AJ, 135, 2453
R Development Core Team. 2010, R: A Language and Environment for Statistical Computing, R Foundation for Statistical Computing, Vienna, Austria, ISBN 3-900051-07-0
Raiteri, C. M., Villata, M., Capetti, A., Heidt, J., Arnaboldi, M., & Magazzù, A. 2007, A&A, 464, 871
Rawlings, S., & Saunders, R. 1991, Nature, 349, 138
Rector, T. A., Stocke, J. T., Perlman, E. S., Morris, S. L., & Gioia, I. M. 2000, AJ, 120, 1626
Sbarufatti, B., Treves, A., & Falomo, R. 2005, ApJ, 635, 173
Stickel, M., Padovani, P., Urry, C. M., Fried, J. W., & Kuehr, H. 1991, ApJ, 374, 431
Swain, M. R., Bridle, A. H., & Baum, S. A. 1998, ApJ, 507, L29
Trussoni, E., Capetti, A., Celotti, A., Chiaberge, M., & Feretti, L. 2003, A&A, 403, 889
Turriziani, S., Cavazzuti, E., & Giommi, P. 2007, A&A, 472, 699
Urry, C. M., & Padovani, P. 1995, PASP, 107, 803
Vermeulen, R. C., Ogle, P. M., Tran, H. D., Browne, I. W. A., Cohen, M. H., Readhead, A. C. S., Taylor, G. B., & Goodrich, R. W. 1995, ApJ, 452, L5+
Wall, J. V., Jackson, C. A., Shaver, P. A., Hook, I. M., & Kellermann, K. I. 2005, A&A, 434, 133
Wall, J. V., & Peacock, J. A. 1985, MNRAS, 216, 173
Wilks, S. 1938, Ann. Math. Statist., 9, 60
Willott, C. J., Rawlings, S., Blundell, K. M., & Lacy, M. 1999, MNRAS, 309, 1017